



**HAL**  
open science

# Multiscale out-of-equilibrium dynamics driven by pulsed laser excitation in spin-crossover materials: A combined thermoelastic and mechanoelastic study

Laurentiu Stoleriu, Masamichi Nishino, Seiji Miyashita, Alexandru Stancu, Roman Bertoni, Eric Collet, Maciej Lorenc, Cristian Enachescu

## ► To cite this version:

Laurentiu Stoleriu, Masamichi Nishino, Seiji Miyashita, Alexandru Stancu, Roman Bertoni, et al.. Multiscale out-of-equilibrium dynamics driven by pulsed laser excitation in spin-crossover materials: A combined thermoelastic and mechanoelastic study. *Physical Review B*, 2023, 108 (1), pp.014306. 10.1103/PhysRevB.108.014306 . hal-04195287

**HAL Id: hal-04195287**

**<https://hal.science/hal-04195287>**

Submitted on 26 Nov 2023

**HAL** is a multi-disciplinary open access archive for the deposit and dissemination of scientific research documents, whether they are published or not. The documents may come from teaching and research institutions in France or abroad, or from public or private research centers.

L'archive ouverte pluridisciplinaire **HAL**, est destinée au dépôt et à la diffusion de documents scientifiques de niveau recherche, publiés ou non, émanant des établissements d'enseignement et de recherche français ou étrangers, des laboratoires publics ou privés.

# Multiscale out-of-equilibrium dynamics driven by pulsed laser excitation in spin-crossover materials: A combined thermoelastic and mechanoelastic study

Laurentiu Stoleriu,<sup>1</sup> Masamichi Nishino<sup>1b</sup>,<sup>2</sup> Seiji Miyashita<sup>1b</sup>,<sup>3,4</sup> Alexandru Stancu,<sup>1</sup> Roman Bertoni<sup>1b</sup>,<sup>4,5</sup> Eric Collet,<sup>4,5</sup> Maciej Lorenc,<sup>4,5</sup> and Cristian Enachescu<sup>1,\*</sup>

<sup>1</sup>*Faculty of Physics, Alexandru Ioan Cuza University of Iasi, Romania*

<sup>2</sup>*Research Center for Advanced Measurement and Characterization, National Institute for Materials Science, 1-1 Namiki, Tsukuba, Ibaraki 305-0044, Japan*

<sup>3</sup>*Department of Physics, Graduate School of Science, The University of Tokyo, 7-3-1 Hongo, Tokyo 113-0033, Japan*

<sup>4</sup>*DYNACOM IRL2015 University of Tokyo - CNRS - URI, Department of Chemistry, 7-3-1 Hongo, Tokyo 113-0033, Japan*

<sup>5</sup>*Univ Rennes, CNRS, UBL, IPR (Institut de Physique de Rennes)- UMR 6251, F-35000 Rennes, France*



(Received 20 November 2022; revised 18 May 2023; accepted 6 July 2023; published xxxxxxxxx)

In this paper, we present an elastic model coupled with a heat propagation process in order to reproduce the out-of-equilibrium dynamics of spin crossover materials driven by femtosecond laser excitation: a multiscale out-of-equilibrium dynamics driven by pulsed laser excitation in spin-crossover materials (thermoelastic step), the thermal switching (thermal step), and the subsequent relaxation to the initial state on cooling. The simulations were performed for open boundaries two and three-dimensional samples, composed of individual molecules linked by springs, which stand for elastic interactions. This building-up of the samples allows the propagation of elastic waves, which leads to accumulation of high spin molecules towards edges at the maximum of the thermoelastic step. We first show that a simple model with a single “temperature” reproduces the thermoelastic, the thermal step and the relaxation to the original equilibrium state. However, the too slow thermalization of the lattice obtained in this model does not correspond to the experimental data. Therefore, to overcome this drawback, we consider either an inhomogeneous photoexcitation or different “temperatures” for the lattice and the spin states. The effect of the sample size, which prevents the existence of a thermal step in the case of nanoparticles is also discussed, as well as the three-dimensional model.

DOI: [10.1103/PhysRevB.00.004300](https://doi.org/10.1103/PhysRevB.00.004300)

## I. INTRODUCTION

Spin crossover systems are metal complexes showing the unique ability to have two metastable spin states, high spin (HS) and low spin (LS), characterized by specific optical and magnetic properties, that can be triggered by using external stimuli, such as temperature, pressure, light [1]. The smaller cohesion energy in the HS state determines longer coordination bond lengths and larger molecular volume. A first consequence of the change of molecular volume is the existence of elastic interactions between the metal ions, which if strong enough, leads to cooperative switching accompanied by a first order phase transition (hysteresis) with temperature, light or pressure as input parameters. This property is important for practical applications, as the information storage. The thermal conversion from LS to HS state occurs at the critical temperature  $T_C$ . The LS state, stable at low temperatures, can be switched towards the long-lifetime metastable HS state by optical excitation of some specific charge transfer or metal-centred bands [2,3], with a light irradiation, by the way of the so called light induced excited spin state trapping (LIESST) effect [4,5]. Pulsed laser irradiation allows the control of this bistability in an ultrafast way, by induc-

ing out-of-equilibrium conditions [6–12]. In solids, the initial femtosecond photoswitching is localized at molecular level for few absorbing molecules towards HS state and triggers a subsequent increase of the fraction of HS molecules at longer time, driven by lattice expansion. This phenomenon is known as thermoelastic step. Recent development of elastic models for spin-crossover materials, which treat the molecular volume variation accompanied by the spin state change and elastic interactions between molecules, has clarified important cooperative properties in spin crossover phenomena [13–20]. It was demonstrated that this cooperative switching occurs due to the propagation of the elastic waves, taking place on the acoustic time scale, which corresponds to the ratio between relevant spatial scale and the sound velocity in the medium [8]. The amplitude of the phenomenon is measured through the HS fraction, which is the proportion of molecules in the HS state, denoted here by  $X_{HS}$ . Yet more spectacular, the elastic step can be followed, for appropriate photoexcitation rates and system sizes, by the so-called thermal step, which is a further increase of  $X_{HS}$ , at a larger timescale due to the propagation of heat deposited by laser excitation throughout the lattice [21].

In order to understand this complex out of equilibrium behavior, where different degrees of freedom equilibrate over different spatial and time scales, we should first clarify the role of independent propagations of elastic waves and heat on the

\*cristian.enachescu@uaic.ro

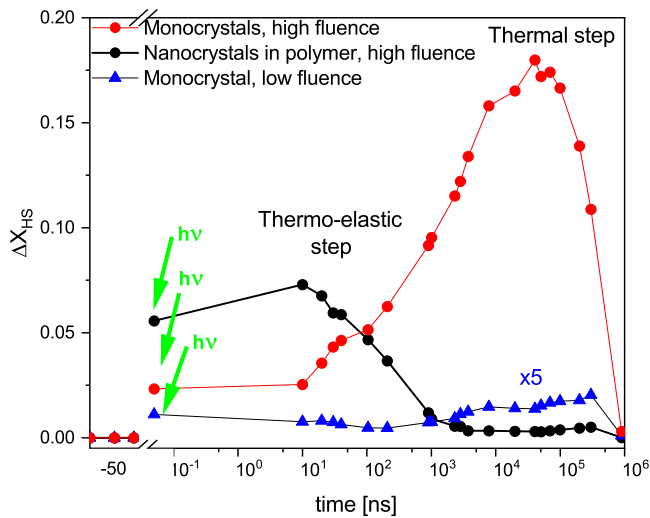


FIG. 1. Photoconversion to femtosecond laser excitation of LS  $[\text{Fe}^{\text{III}}(3\text{-MeO-SalEen})]\text{PF}_6$  in the form of micro- and nanocrystals. “ $h\nu$ ” denotes the photoinduced step, followed by thermoelastic and thermal steps.

recovered within 1  $\mu\text{s}$ ; in some cases a thermal step can be noticed, even in the absence of a thermoelastic step.

The increase of the high spin fraction subsequent to photoexcitation takes place in two steps, as we explain below. During ultrafast laser irradiation, a large amount of energy is locally deposited in every molecule photoexcited from LS to HS state, which causes both the local switching of electronic state and the molecular structural reorganization, together with the coherent and incoherent activation of molecular vibrational modes [23–25]. The LS-HS switching is accompanied by the increase of the molecular volume (metal-ligand distance) within less than 1 ps, which first determines the building-up and then the propagation of elastic interactions between spin crossover molecules within the crystalline lattice. This finally leads to the global lattice expansion, which produces negative lattice pressures on individual molecules, favoring the HS state of higher volume and resulting in a fast switching of more molecules towards HS state through a cooperative elastic process [26]. After this thermoelastic expansion (thermoelastic step), HS fraction decreases for a while. On the other hand, the energy deposited into photoexcited molecules, which far exceeds the amount needed for the LS-HS conversion (20 meV), is transferred to the surrounding lattice through vibrational cooling [27]. The distance between “hot spots (photoexcited sites)” is small for homogeneous excitation: namely, for 4% excitation one molecule over 25 absorb energy, which corresponds to one hot spot in a box of  $3 \times 3 \times 3$  molecules. Therefore the energy redistribution leads to a rapid homogenization (on the order of a dozen of ps) of the temperature of the lattice through molecular vibrations and phonon population [28,29]. This lattice warming can also result in its thermal expansion. However, it should be noted that the high spin state population becomes thermally equilibrated with the lattice in a time of the order of 10  $\mu\text{s}$ , which corresponds to the “thermal step” in Fig. 1, much slower than the thermalization of the lattice. Thus the difference of the time scale of the thermalizations of lattice and spin state plays an important role for the elastic step and the thermal step.

macroscopic spin state switching and what actually represents the notion of temperature. The aim of this paper is to propose a realistic model able to reproduce both elastically-driven and thermally-driven processes, considering the propagation of the elastic interactions producing the local stresses at individual molecules. The paper is organized as follows: first we present relevant experimental data, then we discuss the model, including the concept of different temperatures for the lattice and for the spin state and the simulation of the heat propagation. The main part of the paper is devoted to macroscopic and microscopic data for 2D and 3D samples, showing the effect of various parameters of the system.

## II. RESULTS

### A. Review on experimental data and theoretical concepts

Typical experiments showing the nonlinear response of a spin crossover system to a femtosecond laser excitation are shown in Fig. 1 for  $[\text{Fe}^{\text{III}}(3\text{-MeO-SalEen})]\text{PF}_6$  samples of different sizes, which was reported in detail in Ref. [7]. The fraction of molecules switched by light from LS to HS states, within less than 1 picosecond, depends linearly on the photon excitation density, as one absorbed photon switches one molecule [22]. For higher photoexcitation density (black circles – nanocrystals in polymer, red circles – hundreds of micrometer single crystal; in Fig. 1), a self-amplified transformation towards HS state occurs within 10 ns, which is known as thermoelastic step. In addition to this first amplification, a second amplification is observed after a microseconds time in the case of single crystals (red and blue circles). In the case of nano-crystals (black circles), after the initial self-amplification, the samples relax back to the low temperature equilibrium state and no thermal step is observed. No thermal step was observed in the case of low photoexcitation (blue triangles). When the fraction of photoswitched molecules from LS to HS state is below a threshold, the LS ground state is

### B. Models and discussion

#### 1. The thermo-mechano-elastic model

In order to discuss both elastic and thermal steps in the framework of a unified model, we use here a modified mechanoelastic model, which was previously applied to simulate the elastic self-amplification alone. In this model, the molecules, represented as rigid spheres, are situated in open boundary lattices. The elastic interactions are simulated by springs linking a molecule to its closest neighbors. When a molecule changes its state, its volume varies, which results in an immediate elongation or a compression of its closest springs, determining first the motion of neighboring molecules and then the propagation of the initial perturbation towards all the lattice.

The elastic simulations of spin crossover materials imply two processes: the switch of spins and the change in molecular positions [30]. The spin change may be performed either by the way of Metropolis criterion or by an Arrhenius approach, which is used here, as faster and more appropriate to dynamic phenomena. Because we study local spring interactions

among molecules, the strain effect (elastic interaction) is automatically taken into account,

Therefore every spin change will influence both neighboring and, in a smaller extent, far-away molecules. In this way, a single elastic constant stands for both short-range and long-range interactions.

Most of the simulations in this paper have been performed for a 2D rectangular shape system composed of 13 824 molecules in a triangular configurational bonding. The Arrhenius molecular switching probabilities of the  $i$ th spin between the LS and HS states depend on the “temperature”  $T$ , on intrinsic material parameters (the HS-LS energy difference  $D$ , the degeneracy ratio  $g$ , the effective activation energy  $E_A$ ) and on the effective elastic interactions between molecules, represented here by the way of the local pressure force  $p_i$  acting on molecule  $i$ , and are explicitly given by in the following equations:

$$\begin{aligned} P_{\text{HS} \rightarrow \text{LS}}^i &= \frac{1}{\tau} \exp\left(-\frac{E_A - \kappa p_i}{k_B T_i}\right), \\ P_{\text{LS} \rightarrow \text{HS}}^i &= \frac{1}{\tau} \exp\left(-\frac{D - k_B T_i \ln g}{k_B T_i}\right) \\ &\quad \times \exp\left(-\frac{E_A + \kappa p_i}{k_B T_i}\right), \end{aligned} \quad (1)$$

where  $\tau$  is a constant scaling factor ensuring that the probabilities are below unity, and  $\kappa$  a scaling constant linking the local pressure with the activation energy. We have to strengthen that the local pressure force is the key parameter of the model, as it can dramatically change the steady state of the system. Using a Monte Carlo standard procedure, one decides if a molecule switches or not by comparing its transition probability with a random number  $\eta \in (0, 1)$ . One Monte Carlo electronic step (MCES) is completed when every molecule has been checked once. After every MCES, the new positions of molecules must be found either by the mechanical relaxation of the lattice considering small displacements on all axes, using a Nose-Hoover formalism [20] or, as used here, by computing the motion of molecules solving the following system of differential equations for all molecules:

$$\begin{aligned} m \frac{d^2 x_i}{dt^2} &= F_{i,x} - \mu \frac{dx_i}{dt} \\ m \frac{d^2 y_i}{dt^2} &= F_{i,y} - \mu \frac{dy_i}{dt}, \end{aligned} \quad (2)$$

where  $x_i$  and  $y_i$  are the Cartesian coordinates of the molecule  $i$ ,  $m$  is the mass of the molecule,  $\mu$  is a damping constant, preventing the system to enter into an uncontrolled oscillatory motion, and  $F_{xi}$ ,  $F_{yi}$  are the components of the instantaneous force  $\vec{F}_i$  acting on molecule  $i$  given by the sum of the forces from the neighboring springs.

The number of steps  $r$  to solve the system of coupled differential equations after every MCES is a key ingredient for the transient evolution of the system [26,31]. The value of  $r$ , tunes the different time scales of spin dynamics and lattice relaxation and is a measure for how fast the lattice relaxation is in comparison with individual molecular switching. A large  $r$  favours equilibrium distribution, specific for static phenomena, whereas a smaller  $r$  favours nonequilibrium distribution

as in the case of fast phenomena subsequent to femtoseconds photoexcitation experiments [30].

The steady state of the system before photoexcitation is generated by computing at least 5000 MCES at the given temperature (i.e., at 145 K where most of the simulations have been performed to reach the steady state corresponding to a  $X_{\text{HS}}$  of around 0.06). The material parameters used in simulations, in line with standard experimental calorimetric data for Fe(II) spin crossover systems [32,33], were  $D = 1100$  K,  $g = 1096$ , thus giving a thermal transition temperature  $[D/(k_B \ln(g))]$  of around 157 K. The radius of HS molecules is considered to be 0.22 nm, and that of LS molecules 0.2 nm. The distance between centres of molecules is 1.04 nm for two molecules in HS state and 1 nm for two molecules in LS state. These values correspond to x-ray experimental measurements for typical spin crossover compounds [32,33]. The elastic constant of intermolecular springs is 7 N/m, which generates a moderate cooperativity in the system [34]. As in previous works,  $\kappa$  is taken  $1450 \times 10^{-14} \text{ J/N}$  while  $\tau = 1000 \text{ s}^{-1}$  [11,13].

Photoirradiation randomly transforms more molecules to the HS state in addition to those in the steady state. The temperature of the photoexcited molecules is increased by  $\Delta T = 100$  K. The simulation starts immediately after the first thermalization and deals with the second and third thermalization, as described in the introduction. The heat propagates through the sample following the Fourier’s law of heat conduction:

$$\frac{dQ}{dt} = -k \nabla T \quad (3)$$

with  $k$  denoting the thermal conductivity. Using the continuous equation of the heat and the relation  $Q = \rho c_p T$ , the equation of the distribution of the temperature is written after a few transformations [35] as

$$\frac{dT}{dt} = \frac{k}{\rho c_p} \nabla^2 T = D_T \nabla^2 T, \quad (4)$$

where  $\rho$  is the mass density,  $c_p$  the specific heat at constant pressure and  $D_T$  denotes the thermal diffusion constant.

Equation (4) can be approximately transposed by a finite difference method [35,36], considering two kinds of heat transfer, i.e., the diffusion in the bulk of system and the heat transfer to the bath (external), to the following equation of lattice temperature diffusion:

$$\frac{dT_L^i}{dt} = -\alpha(T_L^i - \langle T_L^i \rangle) - \beta(T_L^i - T_B), \quad (5)$$

where  $T_L^i$  is the lattice temperature of the  $i$ th molecule,  $\langle T_L^i \rangle$  is the average of lattice temperatures for all neighbors of the  $i$ th molecule,  $\alpha$  is the diffusion coefficient,  $T_B$  is the external thermal bath temperature and  $\beta$  is the heat transfer coefficient to the bath. By the second term at the right-hand side, which is considered for only edge molecules, the lattice temperature approaches the bath temperature from the edges to the inner part.

The algorithm for simulations is then completed within the thermoelastic model with the computation of temperatures of every molecule considering Eq. (5), after every update of all the spin state MCES after photoexcitation. Typical



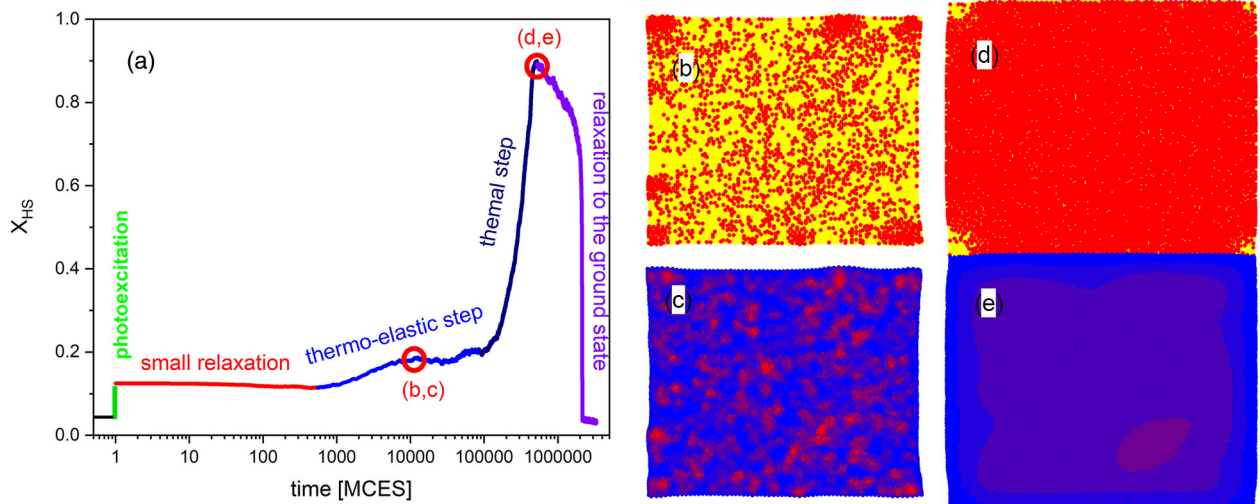


FIG. 2. Evolution of the system after ultrafast photoexcitation showing relaxation, thermoelastic step, thermal step and the final relaxation to the ground state. (a) Snapshots of the system at the maximum of the thermoelastic step [(b) and (c)] and at the maximum of the thermal step [(d) and (e)]. Spin states maps [(b) and (d)]: red circles: HS molecules, yellow circles: LS molecules; down: temperature map). Temperature maps [(c) and (e)] blue: low temperature, red: high temperature

263 results of simulations using Eq. (1) coupled with Eq. (5),  
 264 where  $T_L^i = T_i$  are presented in Fig. 2(a) for coefficients  
 265  $\alpha = 0.0005 \text{ MCES}^{-1}$ ,  $\beta = 0.001 \text{ MCES}^{-1}$ , after 10% photo-  
 266 toexcitation at 145 K. Both the thermoelastic and the thermal  
 267 step were reproduced using these parameters and the distri-  
 268 butions of temperature are marked in the figure with a color  
 269 scale. Just after the photoexcitation, the newly switched HS  
 270 molecules are subject to large local pressures, due to their  
 271 increase in size, which determines the immediate compression  
 272 of neighboring springs. These large pressures determine a  
 273 small relaxation of the system, due the switching back of  
 274 several HS molecules to the lower volume LS state exper-  
 275 imentally reported [7,8]. The subsequent lattice relaxation  
 276 leads to a decreasing of local pressure, which is a trigger  
 277 for the thermoelastic step—the increase in number of HS  
 278 molecules. Because the local pressure is smaller towards  
 279 edges and corners due to geometric considerations (less neigh-  
 280 bors), accumulations of HS molecules (small clusters) mostly  
 281 appear in outer parts of the lattice [Fig. 2(b)]. Later on,  
 282 the energy due the photoexcitation is distributed in the whole  
 283 system and has the effect of the increase of the temperature  
 284 of the whole sample above the critical temperature  $T_C$  and  
 285 a large number of molecules switch to HS state [Figs. 2(d)  
 286 and 2(e)]. However, this slow thermalization over the whole  
 287 lattice is not compatible to the experimental fact that the en-  
 288 ergy is distributed very rapidly to the whole lattice uniformly  
 289 as mentioned above. This problem will be resolved in the  
 290 following. Finally, due to heat transfer to the external bath,  
 291 the temperature in the system slowly decreases to the initial  
 292 one and most of the molecules switch back to their ground LS  
 293 state.

294 As we have discussed in the previous paragraph, all the  
 295 macroscopic phenomena are successfully reproduced within  
 296 the present model. However, in the introductory part, we have  
 297 claimed that the thermalization of the lattice is very fast,  
 298 and happens long time before the thermal step, as discussed  
 299 even in early works concerning the photoinduced molecular

switching [37]. Within this aspect, the results presented in  
 Fig. 2(c) indicates a weakness of the present approach: we  
 notice that at the maximum of the thermoelastic step, the  
 distribution of the temperature in the lattice is very large; ac-  
 tually, the thermalization of the lattice is produced in the same  
 time as the thermal step. In order to avoid this drawback, we  
 propose in the following two alternatives of the current model  
 corresponding to different thermalization processes of differ-  
 ent subsystems. In previous works on ultrafast magnetism,  
 the different thermalization timescales and energy transfert  
 between electron, spin and lattice have been described through  
 different temporal evolution of their respective temperatures.  
 It was shown that they are equilibrated in the irradiated  
 material after a very short time (about 5 ps) [38–41] the  
 photoinduced out-of-equilibrium dynamics in Bismuth was  
 discussed in terms of equilibration of electronic and lattice  
 subsystems [42,43]. In the present work, we use an analogy to  
 describe multiscale thermal equilibration.

## 2. The thermo-mechano-elastic model including a two thermalization sequence

The multiscale out-of-equilibrium dynamics induced by a femtosecond laser pulse in spin crossover materials and the subsequent thermalizations of the different degrees of freedom are different from what occurs in ultrafast magnetism or coherent phonons, for which the energy is deposited on delocalized electrons which thermalize rapidly as heated up by the laser pulse. Indeed, in the case of spin crossover materials, the energy is locally deposited on switched molecules that absorbed photons. We therefore consider different subsystems – the “hot” molecules locally photoswitched from low to high spin state due to optical excitation, the lattice heated up by energy transfert and expanding due to molecular swelling and the spin state of the molecules on the lattice, which equilibrate on a different timescale.

344 The difference between the equilibration times and the  
 345 thermal step times suggests that the conversions driven by  
 346 pressure and by temperature must be of different natures.  
 347 While the local pressure excites the vibration modes implied  
 348 in the volume change during LS-HS switching (spin states  
 349 or breathing modes), the heat is transmitted from the lattice  
 350 to all the vibration modes and, only in a subsequent process  
 351 the spin state equilibrates. Indeed, this degree of freedom  
 352 has longer equilibrations timescale and is therefore frozen  
 353 on short timescales. Consequently, in order that the thermal  
 354 transition takes place, an energy transfert is required from  
 355 the hot lattice to the breathing modes, corresponding to the  
 356 molecular reaction coordinate from LS to HS state, but the  
 357 heated molecule needs enough time to explore the different  
 358 molecular configurations and reach the maximum entropy HS  
 359 state.

360 The difference between the timescales of the lattice ther-  
 361 malization and the macroscopic spin state equilibration with  
 362 the hot lattice can be accounted for in the frame of our  
 363 thermoelastic model by considering two temperatures: the  
 364 “lattice temperature” ( $T_L$ ) which corresponds to all lattice vi-  
 365 bration modes and the “molecular spin state temperature” ( $T_S$ )  
 366 to describe the thermal activation of the breathing vibration  
 367 modes, which is directly connected to the LS-HS switching  
 368 probabilities. We also denote as  $T_S^*$  the initial temperature of  
 369 photoexcited molecules and  $T_B$  the temperature of the external  
 370 thermal bath (cryostat, polymer, etc.) which corresponds to  
 371 the initial (prior to photoexcitation) and final (after the relax-  
 372 ation of the thermal step) temperatures. The energy transfers  
 373 and “temperatures” (we use quotes as the concept of tempera-  
 374 ture, necessary in the model, is different at the level of a single  
 375 molecule) can be summarized as follows [see Fig. 3 (top)].

376 (1) Ultrafast photoexcitation: the light transforms some of  
 377 the LS molecules into hot photoexcited molecules with  $T_S^*$ .

378 (2) Photoexcited molecules release their energy towards  
 379 neighboring lattice: first thermalization within  $t_{ML} \approx 10$  ps  
 380 [7]. After this stage the molecular spin state temperature of  
 381 photoexcited molecules and the lattice temperature are equal:  
 382  $T_S(t_{ML}) = T_L(t_{ML}) = T_B + \Delta T$ , while for the other molecules  
 383  $T_L(t_{ML}) = T_B + \Delta T > T_S(t_{ML})$ , where  $\Delta T$  is the molecular  
 384 temperature jump. It depends on the number of switched  
 385 molecules as  $\Delta T = n_{\text{photon}} \Delta E$ , where  $n_{\text{photon}}$  is the density of  
 386 photoexcited molecules and  $\Delta E$  is the energy injected by a  
 387 photon.

388 (3) Lattice towards spin state: the energy transfert from  
 389 lattice to molecule is responsible for a slower spin state  
 390 switching, which is responsible for slower thermal population  
 391 of the HS state within  $t_{SS} \approx 10 \mu\text{s}$ . In this stage, the spin  
 392 temperature becomes close to the lattice temperature, and  
 393 the conversion from LS to HS at nonphotoexcited molecules  
 394 takes place. After this step, the global thermalization of the  
 395 subsystems is reached with equal temperatures [44].

396 (4) System towards bath: third thermalization within  
 397  $t_B \approx 1 \mu\text{s} - 1 \text{ms}$ . In this step, the energy injected by photoir-  
 398 radiation is released to the bath. This step ensures that the  
 399 “temperatures” of the ensemble reaches the temperature of  
 400 the bath (this time varies as a function of system size, and the  
 401 process takes place from the border to the inner places of the  
 402 sample), so that the system recovers initial equilibrium state  
 403 prior to photoexcitation.

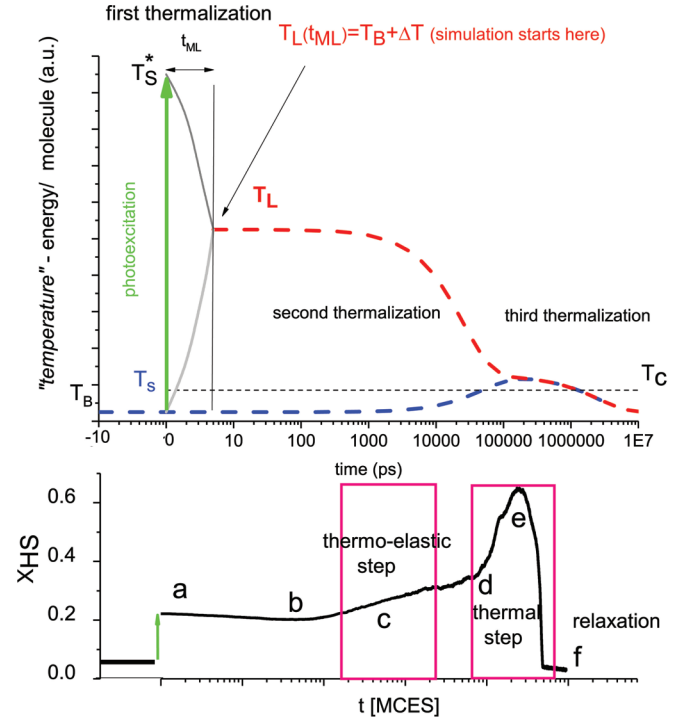


FIG. 3. (Top) Schema for the behavior of the system after ultrafast photoexcitation:  $T_S$ -like, molecular (spin state) temperature, corresponds only to breathing modes;  $T_S^*$  is the temperature of converted molecules just after photoexcitation;  $T_L$ , lattice temperature, corresponds to all vibrational modes,  $T_C$  is the critical temperature. Before excitation, all subsystems have the same temperature, which is the temperature of the bath  $T_B$ . (Bottom) Simulations using the mechanoelastic model for the 2D system and correspondence between the thermalizations and the elastic, thermal step and relaxation towards initial state.

To be in accord with these statements, we need to extend Eq. (5) to describe the equilibration of the spin state through the equilibration of its temperature. Thus we introduce a model in which Eq. (5) is phenomenologically coupled to the equation of temperature diffusion from the lattice towards the breathing (spin state) modes:

$$\frac{dT_S^i}{dt} = -\gamma(T_S^i - T_L^i), \quad (6)$$

where  $\gamma$  is the spin-lattice interaction constant.

Using this model with appropriate values for the thermal coefficients ( $\alpha = 0.005 \text{ MCS}^{-1}$ ,  $\beta = 0.005 \text{ MCS}^{-1}$ ,  $\gamma = 510^{-5} \text{ MCS}^{-1}$ ), we have simulated the evolution of the system presented in Fig. 3 (bottom). Let us analyze the evolution of the system. Only a small spin state relaxation can be observed just after photoexcitation (b mark in Fig. 2); due to the fact that most of the photoexcited molecules are found in a high-pressure environment, some of the HS molecules switch back to the smaller volume LS state. However, the increase of the temperature of the photoexcited molecule due to the laser pulse prevents the switching back of more molecules. The subsequent expansion of the volume of the whole lattice will decrease the pressure on all molecules in the system, therefore a large part of molecules, especially those on edge or corners,



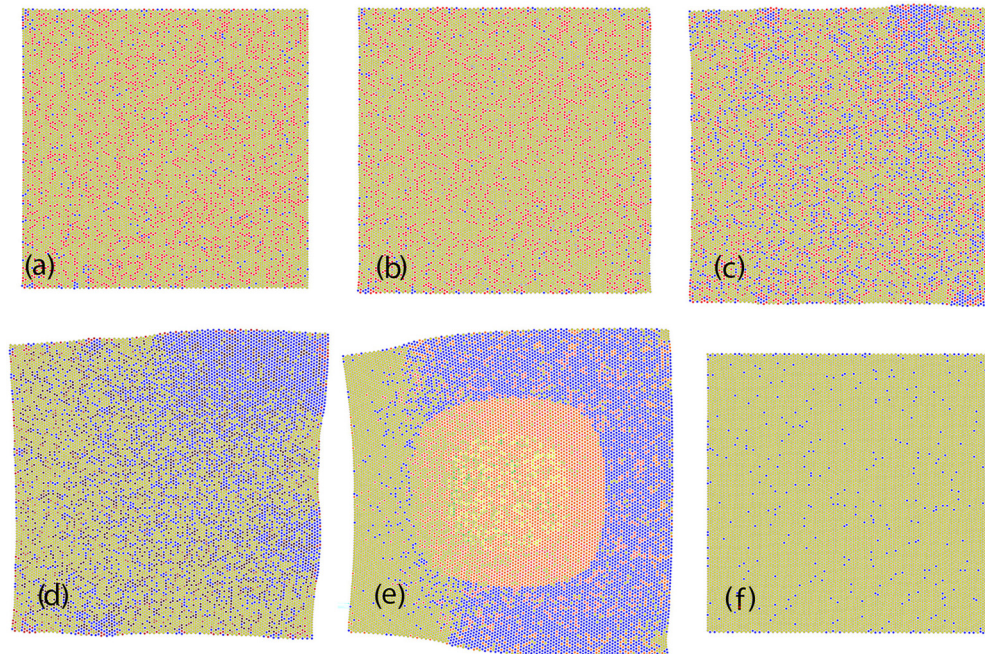


FIG. 4. Snapshots of a 2D system just after photoexcitation (a), during the small relaxation following the photoexcitation (b), at the maximum of the elastic step (c), at the beginning of the thermal step (d), at the maximum of the thermal step (e) and at the end of the final relaxation (f). Yellow: LS molecules, Blue, red, orange: HS molecules (from low to high temperatures, the scale is not the same for all figures). The letters correspond to those marked in Fig. 3, bottom.

415 are in low pressure environment, which helps HS molecules  
 416 to keep their state and LS molecules to switch to HS state. To  
 417 this stage, the molecular spin state temperature stays almost  
 418 constant and the observed effects are of an elastic nature,  
 419 except the role played by the initial increase of temperature,  
 420 as explained above. Therefore this increase of the HS fraction  
 421 has been denoted as elastic or thermoelastic step, because it  
 422 is a thermally activated process, which is driven by elastic  
 423 interactions [7,26]. The next process, observed after a longer  
 424 time, relies on the global evolution of the temperature of the  
 425 spin states in the system as resulting from Eqs. (5) and (6). Its  
 426 significant variation can be detected much later, when it will  
 427 determine the thermal switch of more LS molecules and pro-  
 428 ducing the so-called thermal step. The final stage corresponds  
 429 to the release of all the energy due to photoexcitation in the  
 430 system towards the bath, and system comes back to the initial  
 431 equilibrium state.

432 In Fig. 4, we present snapshots of the system, at different  
 433 instants, before, during and after thermoelastic and thermal  
 434 steps. The molecules are represented as circles with color  
 435 depending on their state and temperatures. In Fig. 4(a), we  
 436 notice the presence of two kinds of HS molecules: blue spins  
 437 with low temperature which are already populated at thermal  
 438 equilibrium at the temperature of the bath  $T_B$  and red (or  
 439 orange) spins with high temperature molecules which are  
 440 switched by the laser. Figure 4(b) shows a configuration just  
 441 after the small relaxation—the lattice volume stays unchanged  
 442 at this step. There, the lattice volume stays unchanged at  
 443 this stage, but due to the high pressure, many of high spins  
 444 are converted to LS, and we see less density of high spins.  
 445 After this high-pressure state, the lattice expands and some  
 446 low spins converted to high spin state in the low pressure

447 due to the expansion. Then, the reorganization of the lattice  
 448 takes place, forming small HS molecules clusters at edges or  
 449 corners, corresponding to the thermoelastic step as depicted  
 450 in Fig. 4(c). After this point, the spin temperature increases  
 451 and many low spins begin to be converted to the high spin  
 452 state. At the beginning of the thermal step [Fig. 4(d)] the  
 453 clusters formed during previous steps develop from corners  
 454 and expand towards the center of the lattice. Figure 4(e) shows  
 455 the configuration at the maximum of thermal step; at this  
 456 stage we notice that the system starts to cool down from the  
 457 edges to central part due to heat flow towards the environment.  
 458 Finally, at the end of the relaxation, the temperature of all  
 459 molecules came back to their initial temperatures, and only  
 460 few molecules thermally populate the HS state at  $T_B$ , below  
 461  $T_C$ . In the system studied here, a local spin state is coupled to  
 462 lattice and patterns of HS and LS molecules appear. Similarly,  
 463 in a ferroelastic system [45], a coupling between strain and  
 464 electrical local dipole moments leads to a pattern formation  
 465 about polarity. Moiré-type patterns on the arrangements of HS  
 466 and LS systems, have been recently observed on thin layers  
 467 of spin crossover systems on substrates in appropriate elastic  
 468 models [46].

469 The dependence of the thermal coefficients on the thermal  
 470 step are presented in Fig. 5. As we explained before, be-  
 471 cause the temperature variation during the thermoelastic step  
 472 is small, these coefficients do not influence the amplitude or  
 473 the position of the thermoelastic step.

474 The role of the internal coefficient  $\gamma$  is explained in Fig. 5  
 475 (top). When  $\gamma$  is large, the relaxation of  $T_S$  to  $T_L$  is fast,  
 476 and thus the displacement of the thermal step appears at smaller  
 477 values of the time. If the  $\gamma$  value is extremely large, the  
 478 thermal step merges with the thermoelastic step. Reversely, a

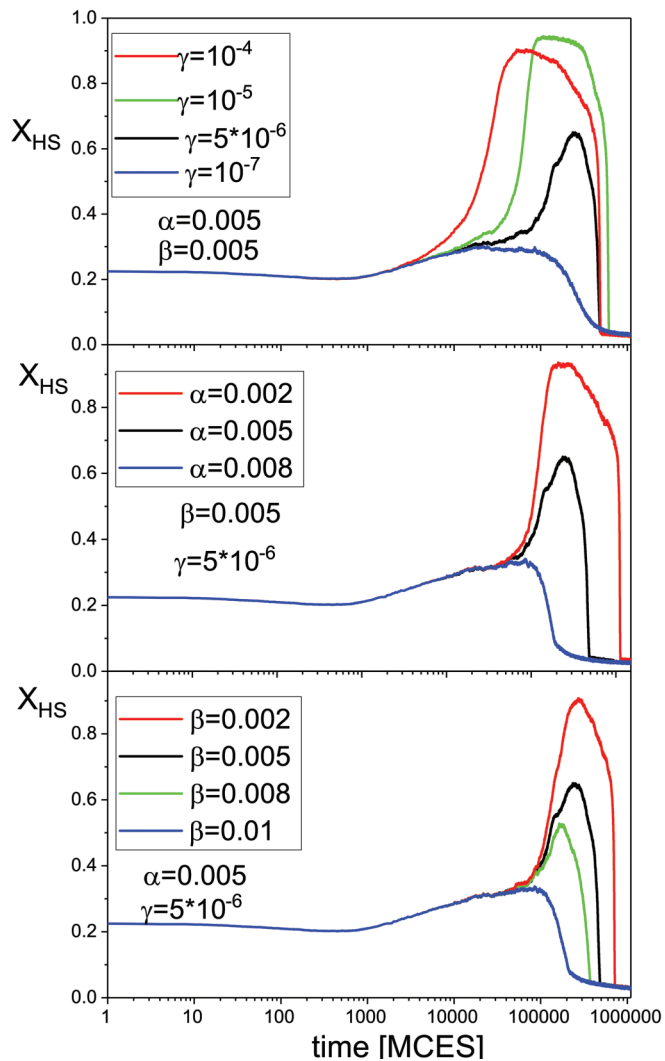


FIG. 5. Dependence of time evolution of  $X_{HS}$  on coefficients (top)  $\gamma$ , (middle)  $\alpha$ , and (bottom)  $\beta$ .

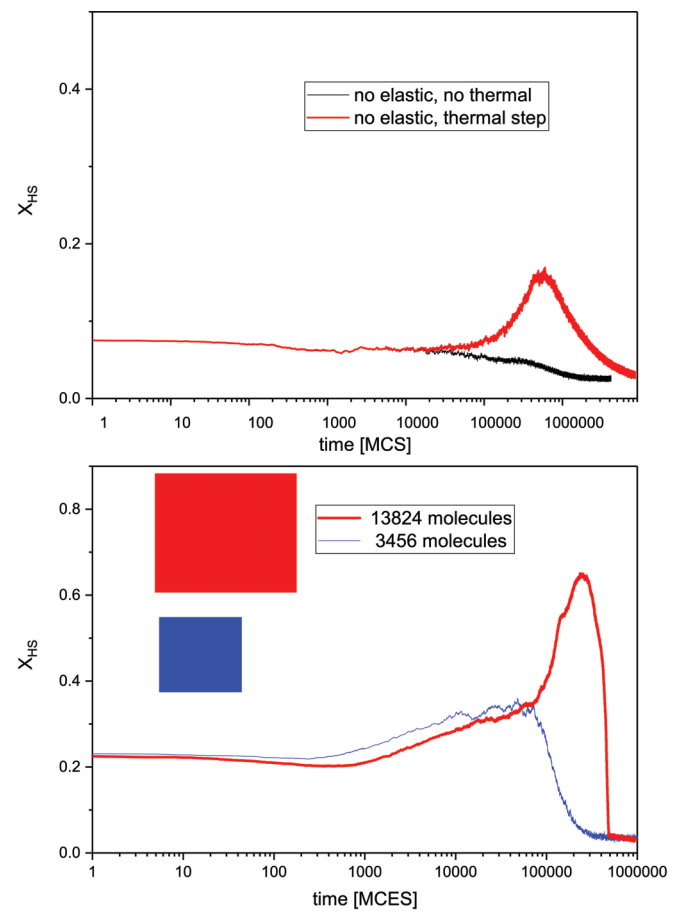


FIG. 6. (Top) Dependence on the amount of photoexcitation. No elastic step and no thermal step take place (if the amount of energy transferred to the lattice is low). No elastic step, but thermal step takes place (for a higher amount of energy inside the lattice). (Bottom) Size effects: the thermal step is observed only in the case of a larger system, for which the exchange with the thermal bath is slower.

479 small  $\gamma$  changes the molecular spin state temperature slower  
 480 than the heat is lost towards the thermal bath, and, conse-  
 481 quently, no thermal step is detected. The effect of thermal  
 482 diffusion coefficients  $\alpha$  and heat transfer coefficient  $\beta$  are  
 483 analysed [Fig. 5(middle and bottom)] and found to be quite  
 484 similar. For larger values of  $\alpha$  and  $\beta$  no thermal step is  
 485 observed, which can be explained with data in Fig. 3 (top): the  
 486 thermal step occurs when the spin temperature becomes larger  
 487 than the transition temperature  $T_C$ . For larger values of  $\alpha$  and  
 488  $\beta$ , the decrease of molecular spin state temperature towards  
 489 the bath is faster than its increase due to the energy received  
 490 from the hot molecules via the lattice, so it does not reach the  
 491 necessary  $T_C$ . Reversely, a larger thermal step is found for a  
 492 slight change of the heat exchange with the bath, when the  
 493 energy of hot molecules has the time to be transformed into  
 494 internal energy of individual molecules.

495 Dependence on the amount of photoexcitation and on the  
 496 size of the lattice are shown in Fig. 6. A smaller initial  
 497 photoexcitation percentage (for example, obtained if using  
 498 lower excitation density) does not allow the building up of the  
 499 thermoelastic step. However, if the energy deposited initially

500 on photoexcited molecules is high enough, then the temper-  
 501 ature of the whole lattice increases enough in order to allow  
 502 the presence of the thermal step, as experimentally shown in  
 503 Fig. 1 for the smaller laser power. A trivial case of neither  
 504 thermoelastic step nor thermal steps may be also obtained in  
 505 experiments. The effect of a small size of the crystal which  
 506 evacuate too fast the heat was also discussed in Ref. [12].

507 In Fig. 6 (bottom), we present the size effects, simulating  
 508 the behavior of two systems with different sizes (13 824 and  
 509 3456 molecules), while keeping all other parameters in the  
 510 system the same. In a smaller sample the heat escape to  
 511 exchange with the bath is faster, and thus, in small samples,  
 512 the temperature will not surpass the critical temperature. This  
 513 corresponds to experimental data shown in Fig. 1, where the  
 514 thermal step is observed only in the case of crystals, and there  
 515 is no thermal step in nanoparticles. In addition, we notice  
 516 that in the case of the small sample the height of the elastic  
 517 step has the same value as in the case of the large sample,  
 518 but it shifts towards shorter times. This is due to the fact  
 519 that in a smaller sample the elastic wave reaches sooner the  
 520 borders of the sample. For the same reason, the relaxation  
 521 after photoexcitation is less intense.



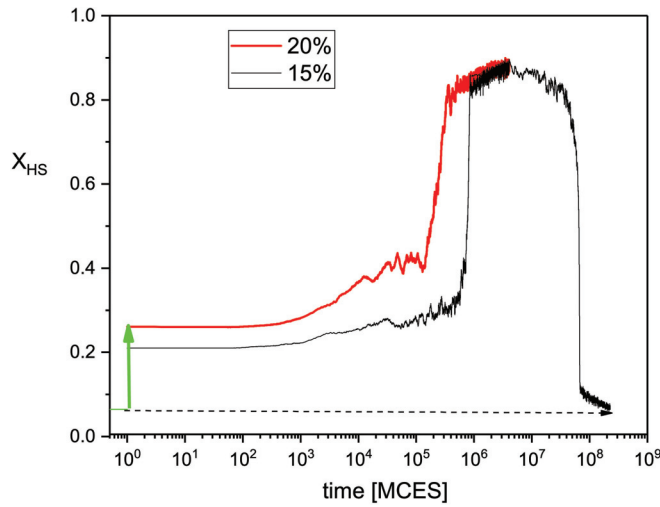


FIG. 7. Simulations using the mechanoelastic model for the 3D system for two initial photoexcitation rates.

3. 3D simulations of the two thermalization scales model

The 2D models can be considered to give a reasonable approximation for conceptual understanding of the phenomena, especially for layered spin crossover compounds with small interactions between the layers. However, several spin crossover systems present a three-dimensional structure, with

the strength of interactions between planes on the same order as within planes and therefore it is important to extend the model towards 3D systems. Due to difficulties related to complexity of the system and the increased number of molecules, less studies have been devoted to modeling 3D systems except some works with open boundaries [47–49] or on surfaces [50–52]. In this section we use a rectangular cuboid system composed of 11 layers of molecules in a face-centred-cubic configuration. Each layer is composed of 1900 molecules in a triangular configuration; every bulk molecule is linked to its twelve closest neighboring molecules (six on the same plane, three below and three above) by springs; molecules on surface layers and those situated on the edge have less neighbors. The probabilities and the thermal diffusion equations are similar as for the 2D case; we have to note that in the 3D systems the molecules are allowed to move outside their initial planes to produce more favourable energetic conditions, leading to so-called buckling effects [47], which have been treated in previous papers for 3D systems of various shapes [48] or for monolayers of spin crossover molecules on substrates, leading to moiré patterns [46]. In Fig. 7, we present the whole curves obtained after 15% and 20% percentage photoexcitation, using the following transfer coefficient parameters  $\alpha = 5 \times 10^{-7} \text{ MCES}^{-1}$ ,  $\beta = 5 \times 10^{-7} \text{ MCES}^{-1}$ , and  $\gamma = 10^{-6} \text{ MCES}^{-1}$ . As in the case of 2D systems we notice the well-defined presence of both the thermoelastic and thermal step. The amplitude of the thermoelastic step is larger

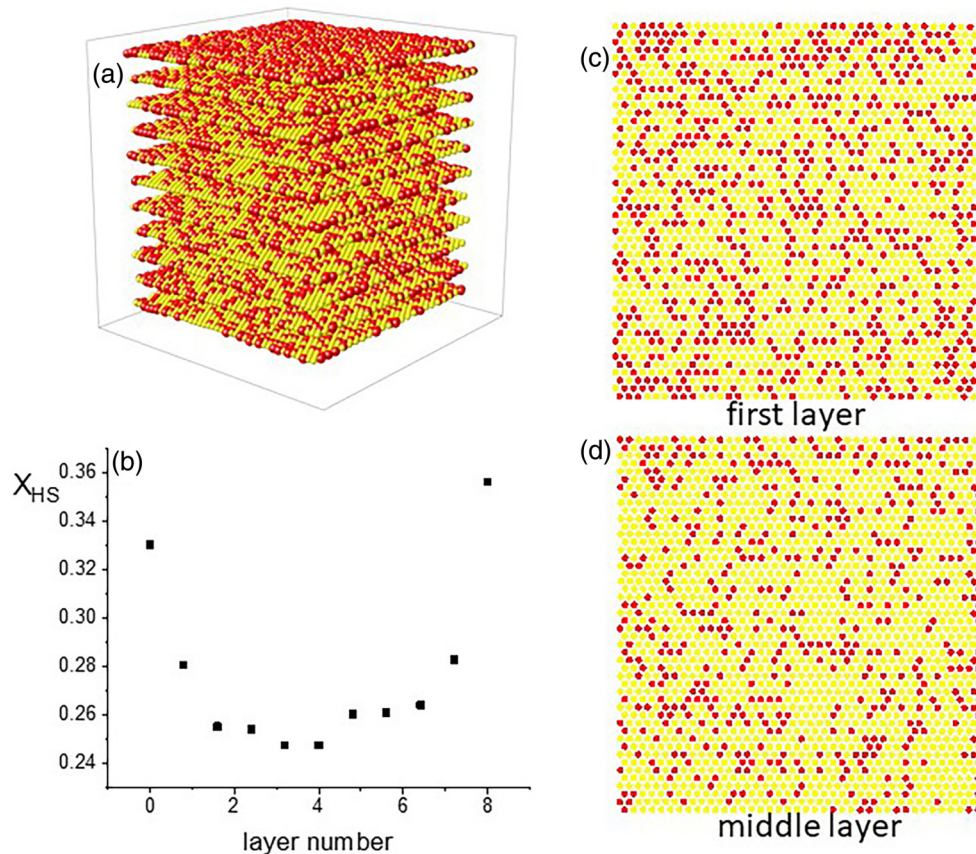


FIG. 8. A snapshot of 3D system at the maximum of the elastic step (a), snapshots of the first (c) and middle layer (d). The dependence of  $X_{HS}$  on the position of layers are shown in (b).

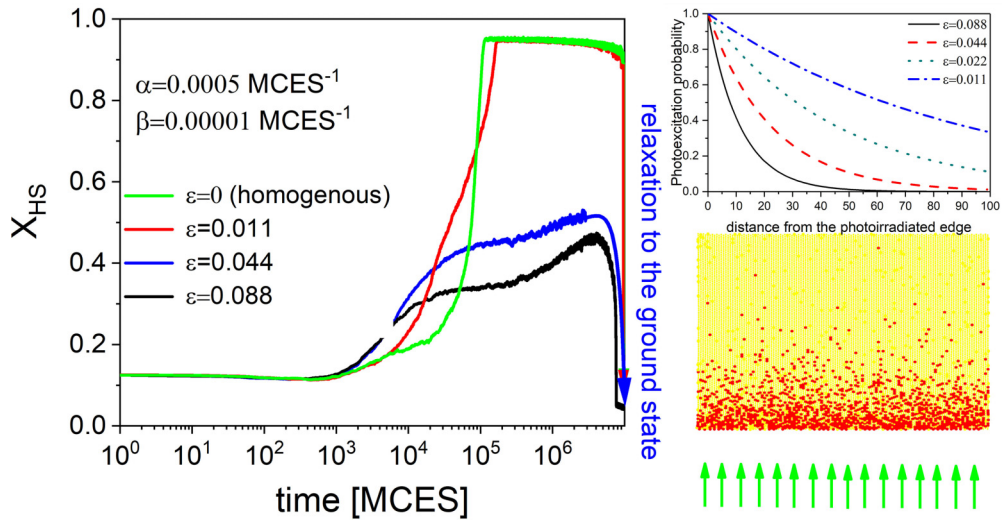


FIG. 9. (Left) Evolution of the system after photoexcitation for different light absorptions (right) Decrease of the photoexcitation probabilities with  $x$  for different absorption coefficients  $\epsilon$ . Snapshot of the system after photoexcitation for  $\epsilon = 0.088$ .

555 in the case of higher initial photoexcitation, as previously  
 556 observed in experiments [7] and simulations [10].

557 We refer now to the configuration of the system during the  
 558 thermoelastic step. As specified above, in a 2D system a re-  
 559 organization of the molecules in the system is observed at the  
 560 maximum of the elastic step, consisting of the accumulation  
 561 of HS molecules towards edges and corners. We analyze here  
 562 the molecular configuration at the maximum of the elastic step  
 563 for a 3D configuration. In Fig. 8(a), we present a snapshot of  
 564 the whole system after 30000 MCS, while the snapshots of the  
 565 first and middle layers are presented in Fig. 8(c) and respec-  
 566 tively Fig. 8(d). At first sight, we notice a higher proportion  
 567 of HS molecules in the first layer comparing to the middle  
 568 layer. A quantitative analysis showing the  $X_{HS}$  for every layer  
 569 is presented in Fig. 8(b) and confirms the initial observation:  
 570 there are more HS molecules in the layers near the surface  
 571 and their number decreases in the layers situated towards the  
 572 center of the sample. Therefore we can conclude that in 3D

systems the molecular reorganization is similar to the one  
 visible in 2D systems.

#### 4. The case of inhomogenous photoexcitation

575 In this section, we refer to the simple thermo-mechano-  
 576 elastic model, including only the lattice temperature, but we  
 577 consider an inhomogenous photoexcitation, which can be ex-  
 578 pected in the case of sample with size of the order or larger  
 579 than the light penetration depth. The photoexcitation probab-  
 580 ility can be written as  $P = \exp(-\epsilon x)$ , where  $\epsilon$  is the absorp-  
 581 tion coefficient and  $x$  is the distance of a molecule from the front  
 582 of irradiation. The effect of the absorption coefficient on the  
 583 distribution of the photoexcited molecules is depicted in the  
 584 right panel of the Fig. 9. In the same figure, we present the  
 585 evolution of the system keeping constant the heat transfer  
 586 parameters and varying the absorption coefficient. We find  
 587 that the homogenous case ( $\epsilon = 0$ ) gives a similar dependence  
 588

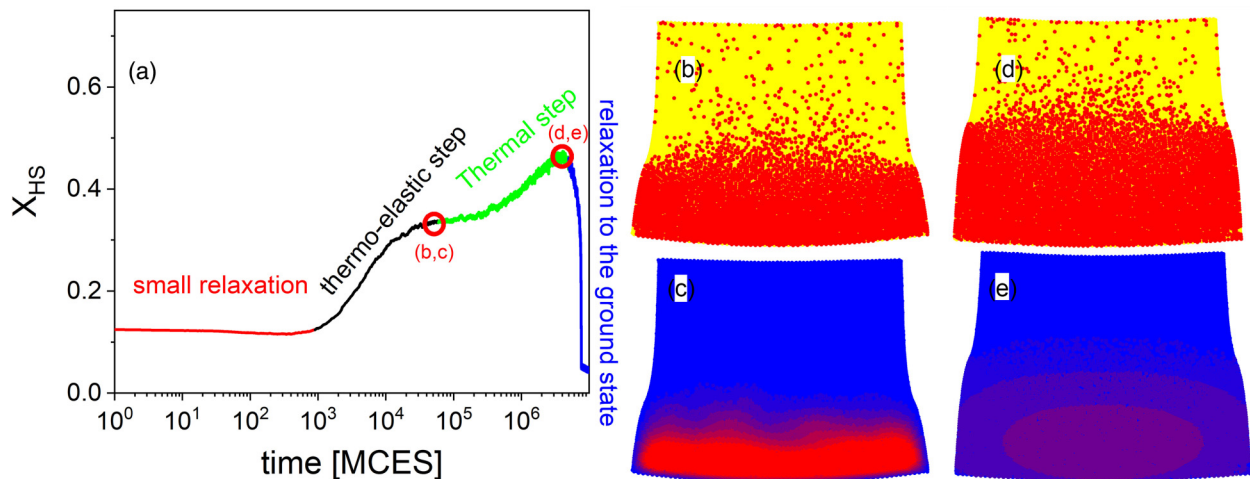


FIG. 10. (Left) Evolution of the  $X_{HS}$  after photoexcitation for  $\epsilon = 0.088$  (a). Snapshots of the system at the maximum of the thermoelastic step [(b) and (c)] and at the maximum of the thermal step [(d) and (e)], spin states map [(b) and (d)], and temperature map [(c) and (e)], using the same scale as in Fig. 2.

to that presented in Fig. 3. If the absorption is present ( $\varepsilon \neq 0$ ), then a clearer disentangling between thermoelastic and elastic steps begins to be visible. Let us refer now to the case when  $\varepsilon = 0.88$  which is presented in Fig. 10. In this situation both the thermoelastic step and the thermal step are well separated, the amplitude of the elastic step is larger, while the amplitude of the thermal step is smaller than in Fig. 2, which correspond to experimental data. Actually, in some previous paper [7,10], the height of the simulated thermoelastic was smaller than the experimental one, so an inhomogenous photoexcitation could approach the simulated data to the experimental ones.

In the right panel of Fig. 10, we present snapshots of the system at the maximum of the thermoelastic step and during the thermal step. Unlike in the homogenous case, in the situation of an inhomogenous photoexcitation, the thermalization of the lattice is already realized at the maximum of the elastic step. The sample is then divided into two distinct parts, with different spin states and temperature. Later on, the temperature will propagate to the rest of the sample, causing the gradual transition of other LS molecules to HS state, which is the thermal step. The increase of the temperature will be however attenuated due to the bath and therefore, the amplitude of the thermal step will be smaller.

### III. CONCLUSIONS

In this paper, in the framework of the 2D and 3D mechanoelastic models considering the heat transfer between thermal bath, lattice and molecular spin state subsystems, we have successfully reproduced both the thermoelastic and the thermal increase of HS population after femtosecond photoexcitation. The out-of-equilibrium dependences of HS fraction evolution  $X(t)$  on the strength of irradiation and also on the size of system are systematically studied, i.e., the faster release of heat to the bath in the case of smaller systems is responsible for the absence of the thermal step which agrees with the observation in the case of nanoparticles in experiment. The present results, dealing with out-of-equilibrium thermalization and heat exchange between subsystems show that describing a complete out-of equilibrium dynamics from local molecular scale to macroscopic scale is complex. In addition to equilibration between subsystems propagating (elastic waves) and diffusive (heat) phenomena must be taken into account. Equally, a most realistic study should consider the propagation of the heat by avalanches of more

correlated regions, as it was theoretical stated in a review on the crackling noise in crystals, ferroelastic and porous materials [53]. Within this aspect, it would be interesting to determine a possible power law function describing the current multiscale phenomena. Similar approaches can be applied for other molecular systems with fast temperature variations or for spin crossover systems heated by plasmonic nanodevices [54]. It should be also noted that in the current method, the spin-transition is done by Monte Carlo sampling. Here we assume that the spin transition itself is much faster than the time scale of lattice motion. The spin transitions occur by contact with the thermal bath. Thus the comparison between the time scale of lattice motion and the that of contact with the bath. In principle, the ratio may result in different aspects of dynamics. This problem was studied by Nishino *et al.* [30], but so far, in our recent works, we used the present scheme to catch general aspects of dynamical phenomena. In the Monte Carlo simulations, the effect of degeneracies of HS and LS is treated in a thermodynamic approach, but not in a dynamical way. This must be investigated more carefully in the future. In principle, we may study the spin transition in the relation of lattice dynamics [55], but several fundamental problems remain to be studied. Thus, in particular for studies of dynamical properties, we should keep in mind these problems. But we still believe that the present work captures many important aspects of the system.

### ACKNOWLEDGMENTS

The authors thank professor Hervé Cailleau for fruitful discussions during the manuscript preparation. This work was supported by a grant of the **Romanian Ministry of Research, Innovation and Digitization, CNCS/CCCDI-UEFISCDI**, Project No. **PN-III-P4-ID-PCE-2020-1946**, within PNCDI III. The authors gratefully acknowledge **Agence Nationale de la Recherche** for financial support undergrant, **ANR-19-CE30-0004 ELECTROPHONE**, **ANR-19-CE29-0018 MULTICROSS**. E.C. thanks the University Rennes 1 and the Fondation Rennes1 for funding. The present work was supported by the **Elements Strategy Initiative Center for Magnetic Materials (ESICMM)** (Grant No. **12016013**) funded by the **Ministry of Education, Culture, Sports, Science and Technology (MEXT)** of Japan, and was partially supported by Grants-in-Aid for Scientific Research C (Grant No. **18K03444** and No. **20K03809**) from **MEXT**.

[1] P. Gütllich and A. Goodwin, *Spin Crossover in Transition Metal Compounds* (Springer, Heidelberg, 2004), Vols. I–III  
 [2] S. Zerdane, L. Wilbraham, M. Cammarata, O. Iasco, E. Riviere, M. L. Boillot, I. Ciofini, and E. Collet, *Chem. Sci.* **8**, 4978 (2017).  
 [3] A. Marino, P. Chakraborty, M. Servol, M. Lorenc, E. Collet, and A. Hauser, *Angew. Chem. Int. Ed.* **53**, 3863 (2014).  
 [4] S. Decurtins, P. Gütllich, C. P. Kohler, H. Spiering, and A. Hauser, *Chem. Phys. Lett.* **105**, 1 (1984).  
 [5] A. Hauser, *Top. Curr. Chem.* **234**, 155 (2004).  
 [6] E. Collet, L. Henry, L. Pineiro-Lopez, L. Toupet, and J. Real, *CIC* **6**, 61 (2016).

[7] R. Bertoni, M. Lorenc, H. Cailleau, A. Tissot, J. Laisney, M. Boillot, L. Stoleriu, A. Stancu, C. Enachescu, and E. Collet, *Nat. Mater.* **15**, 606 (2016).  
 [8] R. Bertoni, M. Lorenc, T. Graber, R. Henning, K. Moffat, J. Letard, and E. Collet, *Cryst. Eng. Comm.* (2016).  
 [9] E. Collet, N. Moisan, C. Balde, R. Bertoni, E. Trzop, C. Laulhe, M. Lorenc, M. Servol, H. Cailleau, A. Tissot, M. L. Boillot, T. Graber, R. Henning, P. Coppens, and M. Buron-Le Cointe, *Phys. Chem. Chem. Phys.* **14**, 6192 (2012).  
 [10] C. Enachescu, L. Stoleriu, M. Nishino, S. Miyashita, A. Stancu, M. Lorenc, R. Bertoni, H. Cailleau, and E. Collet, *Phys. Rev. B* **95**, 224107 (2017).



- [11] R. Bertoni, E. Collet, H. Cailleau, M. L. Boillot, A. Tissot, J. Laisney, C. Enachescu, and M. Lorenc, *Phys. Chem. Chem. Phys.* **21**, 6606 (2019).
- [12] K. Ridier, A. C. Bas, V. Shalabaeva, W. Nicolazzi, L. Salmon, G. Molnar, A. Bousseksou, M. Lorenc, R. Bertoni, E. Collet, and H. Cailleau, *Adv. Mater.* **31**, 1901361 (2019).
- [13] A. I. Popa, L. Stoleriu, and C. Enachescu, *J. Appl. Phys.* **129**, 131101 (2021).
- [14] A. Slimani, K. Boukheddaden, and K. Yamashita, *Phys. Rev. B* **92**, 014111 (2015).
- [15] W. Nicolazzi, S. Pillet, and C. Lecomte, *Phys. Rev. B* **78**, 174401 (2008).
- [16] M. Nishino, K. Boukheddaden, Y. Konishi, and S. Miyashita, *Phys. Rev. Lett.* **98**, 247203 (2007).
- [17] Y. Konishi, H. Tokoro, M. Nishino, and S. Miyashita, *Phys. Rev. Lett.* **100**, 067206 (2008).
- [18] M. Nishino, Y. Singh, K. Boukheddaden, and S. Miyashita, *J. Appl. Phys.* **130**, 141102 (2021).
- [19] C. Enachescu, L. Stoleriu, A. Stancu, and A. Hauser, *Phys. Rev. Lett.* **102**, 257204 (2009).
- [20] C. Enachescu and W. Nicolazzi, *Comptes Rendus Chimie* **21**, 1179 (2018).
- [21] R. Bertoni, M. Lorenc, A. Tissot, M. L. Boillot, and E. Collet, *Coordination Chemistry Reviews* **282-283**, 66 (2015).
- [22] C. Enachescu, U. Oetliker, and A. Hauser, *J. Phys. Chem. B* **106**, 9540 (2002).
- [23] S. Zerdane, E. Collet, X. Dong, S. F. Matar, H. F. Wang, C. Desplanches, G. Chastanet, M. Chollet, J. M. Glowonia, H. T. Lemke, M. Lorenc, and M. Cammarata, *Chem. Eur. J.* **24**, 5064 (2018).
- [24] M. Cammarata, R. Bertoni, M. Lorenc, H. Cailleau, S. Di Matteo, C. Mauriac, S. F. Matar, H. Lemke, M. Chollet, S. Ravy, C. Laulhé, J. F. Létard, and E. Collet, *Phys. Rev. Lett.* **113**, 227402 (2014).
- [25] R. Field, L. C. Liu, W. Gawelda, C. Lu, and R. J. D. Miller, *Chem. Eur. J.* **22**, 5118 (2016).
- [26] A. Volte, C. Mariette, R. Bertoni, M. Cammarata, X. Dong, E. Trzop, H. Cailleau, E. Collet, M. Levantino, M. Wulff, J. Kubicki, F. L. Yang, M. L. Boillot, B. Corraze, L. Stoleriu, C. Enachescu, and M. Lorenc, *Commun. Phys.* **5**, 10.1038/s42005-022-00940-0, 168 (2022).
- [27] M. von Allmen and A. Blatter, *Laser-Beam Interactions with Materials* (Springer, 1995).
- [28] P. Ruello and V. E. Gusev, *Ultrasonics* **56**, 21 (2015).
- [29] A. Marino, M. Cammarata, S. F. Matar, J. F. Letard, G. Chastanet, M. Chollet, J. M. Glowonia, H. T. Lemke, and E. Collet, *Struct. Dyn.* **3**, 023605 (2016).
- [30] M. Nishino, T. Nakada, C. Enachescu, K. Boukheddaden, and S. Miyashita, *Phys. Rev. B* **88**, 094303 (2013).
- [31] M. Nishino, C. Enachescu, S. Miyashita, P. A. Rikvold, K. Boukheddaden, and F. Varret, *Sci. Rep.* **1**, 162 (2011).
- [32] E. König, *Structure and Bonding* **76**, 51 (1991).
- [33] P. Gütllich, A. Hauser, and H. Spiering, *Angew. Chem. Int. Ed. Engl.* **33**, 2024 (1994).
- [34] C. Enachescu and A. Hauser, *Phys. Chem. Chem. Phys.* **18**, 20591 (2016).
- [35] D. Sands, Pulsed laser heating and melting, in *Heat Transfer - Engineering Applications*, edited by IntechOpen (2011).
- [36] V. A. Shneidman and M. C. Weinberg, *J. Non-Cryst. Solids* **194**, 145 (1996).
- [37] H. Cailleau, M. Lorenc, L. Guerin, M. Servol, E. Collet, and M. Buron-Le Cointe, *Acta Crystallogr A Found Crystallogr* **66**, 189 (2010).
- [38] E. Beaupaire, J. C. Merle, A. Daunois, and J. Y. Bigot, *Phys. Rev. Lett.* **76**, 4250 (1996).
- [39] B. Koopmans, G. Malinowski, F. D. Longa, D. Steiauf, M. Faehnle, T. Roth, M. Cinchetti, and M. Aeschlimann, *Nat. Mater.* **9**, 259 (2010).
- [40] D. Zahn, F. Jakobs, Y. W. Windsor, H. Seiler, T. Vasileiadis, T. A. Butcher, Y. P. Qi, D. Engel, U. Atxitia, J. Vorberger, and R. Ernstorfer, *Phys. Rev. Res.* **3**, 023032 (2021).
- [41] J. Kimling, J. Kimling, R. B. Wilson, B. Hebler, M. Albrecht, and D. G. Cahill, *Phys. Rev. B* **90**, 224408 (2014).
- [42] T. Garl, E. G. Gamaly, D. Boschetto, A. V. Rode, B. Luther-Davies, and A. Rouse, *Phys. Rev. B* **78**, 134302 (2008).
- [43] Y. Giret, A. Gellé, and B. Arnaud, *Phys. Rev. Lett.* **106**, 155503 (2011).
- [44] M. Lorenc, C. Balde, W. Kaszub, A. Tissot, N. Moisan, M. Servol, M. Buron-Le Cointe, H. Cailleau, P. Chasle, P. Czarnecki, M. L. Boillot, and E. Collet, *Phys. Rev. B* **85**, 054302 (2012).
- [45] H. Yokota, C. R. S. Haines, S. Matsumoto, N. Hasegawa, M. A. Carpenter, Y. Heo, A. Marin, E. K. H. Salje, and Y. Uesu, *Phys. Rev. B* **102**, 104117 (2020).
- [46] A. Railean, M. Kelai, A. Bellec, V. Repain, M.-L. Boillot, T. Mallah, L. Stoleriu, and C. Enachescu, *Phys. Rev. B* **107**, 014304 (2023).
- [47] K. Boukheddaden and A. Bailly-Reyre, *Europhys. Lett.* **103**, 26005 (2013).
- [48] L. Stoleriu, M. Nishino, S. Miyashita, A. Stancu, A. Hauser, and C. Enachescu, *Phys. Rev. B* **96**, 064115 (2017).
- [49] N. di Scala, N. E. I. Belmouri, M. A. P. Espejo, and K. Boukheddaden, *Phys. Rev. B* **106**, 014422 (2022).
- [50] T. Delgado, C. Enachescu, A. Tissot, L. Guenee, A. Hauser, and C. Besnard, *Phys. Chem. Chem. Phys.* **20**, 12493 (2018).
- [51] M. Kelai, V. Repain, A. Tauzin, W. B. Li, Y. Girard, J. Lagoute, S. Rousset, E. Otero, P. Sainctavit, M. A. Arrio, M. L. Boillot, T. Mallah, C. Enachescu, and A. Bellec, *J. Phys. Chem. Lett.* **12**, 6152 (2021).
- [52] K. Affes, A. Slimani, Y. Singh, A. Maalej, and K. Boukheddaden, *J. Phys.: Condens. Matter* **32**, 255402 (2020).
- [53] E. K. H. Salje and K. A. Dahmen, in *Annual Review of Condensed Matter Physics*, edited by J. Langer (2014), Vol. 5, pp. 233–254.
- [54] Y. W. Hu, M. Picher, N. M. Tran, M. Palluel, L. Stoleriu, N. Daro, S. Mornet, C. Enachescu, E. Freysz, F. Banhart, and G. Chastanet, *Adv. Mater.* **33**, 2105586 (2021).
- [55] M. Nishino, K. Boukheddaden, and S. Miyashita, *Phys. Rev. B* **79**, 012409 (2009).